

# Nonlinear Evolutionary PDE-Based Refinement of Optical Flow

Hirak Doshi, N. Uday Kiran

## Abstract

The goal of this paper is to propose a unified framework for nonlinear refinement of optical flow. The first model is a two-phase refinement process where an initial estimate obtained in the first phase is subsequently refined in the second phase using additional constraints. We study the mathematical well-posedness of this formulation using an evolutionary-PDE approach. The second model is a single-phase improvement process involving an anisotropic regularization of the curl of the flow. For implementation we use the first-order primal-dual Chambolle-Pock algorithm. We observe that the results obtained by both methods are comparable in nature. We perform several numerical experiments and empirically demonstrate that by using a two-phase refinement process, a faster convergence rate of the order  $O(1/N)$  is achieved than the single-phase process which has a higher convergence rate of the order  $O(1/N^2)$ .

**Keywords.** Optical Flow, Evolutionary PDE, Variational Methods, Primal-Dual, Convergence

## 1 Introduction

Optical flow plays a key role in many advanced Computer Vision applications. It is a rich source of information on perceptible motion in our visual world. It's reliable estimation is thus important and at the same time challenging. Assuming the principle of local conservation of intensity and small temporal variations, optical flow involves the recovery of a function  $\mathbf{u} = (u, v)$  such that

$$f(\mathbf{x}, \tau) = f(\mathbf{x} + \mathbf{u}, \tau + \Delta\tau).$$

where  $f : \Omega \times [0, T] \rightarrow \mathbb{R}$  if the image sequence,  $\Omega \subset \mathbb{R}^2$  is open and bounded. This establishes a correspondence between pixel motions. Using first-order approximations the above relation can be written as

$$f_\tau + \nabla f \cdot \mathbf{u} = 0, \quad (1)$$

which is widely known as the Optical Flow Constraint (OFC). To recover the velocity components using a variational minimization approach one writes (1) as

$$\min_{\mathbf{u}} J_1(\mathbf{u}) = \int_{\Omega} (f_t + \nabla f \cdot \mathbf{u})^2.$$

This is the simplest least-square minimization. This problem is ill-posed as it leads to the aperture problem. Additional regularization terms are necessary to ensure well-posedness. The most common regularization term is the quadratic smoothness penalizing the gradient of the components of the flow originally introduced by Horn and Schunck [22] in their seminal work. Cohen [11] and Kumar et.al. [23] used the  $L^1$  regularization which is more robust to outliers and preserves important edge information. A new discontinuity preserving optical flow model with  $L^1$  norm on the OFC was proposed and studied by Aubert et. al. [3] in the space of functions of bounded variations  $BV(\Omega) \times BV(\Omega)$ . The well-posedness of the Horn and Schunck model, as well as the Nagel model was studied by Schnörr [28] in the space  $H^1(\Omega) \times H^1(\Omega)$ . Taking a step further, the authors in [8] proposed a  $L^p - TV/L^p$  ( $p = 1$  or  $2$ ) model combining both  $L^1$  and  $L^2$  terms. The behaviour of their regularization term is similar to the Huber function:

$$H(x; \epsilon) = \begin{cases} \frac{x^2}{2\epsilon}, & 0 \leq |x| \leq \epsilon \\ |x| - \frac{\epsilon}{2}, & |x| > \epsilon. \end{cases}$$

A detailed review and rigorous analysis of several variational optical flow models within the framework of calculus of variations can be found in [21].

Though most of the estimation involving rigid or quasi-rigid motion can be handled by minimizing OFC with a suitable regularization, it is insufficient to provide an accurate estimation for fluid-based images. Traditional computer vision techniques may not be suitable to capture these deformations of brightness patterns because of the high spatio-temporal turbulence in these sequences. These reasons have motivated researchers to look for an alternate constraint that can not only preserve pixel-correspondence but also capture certain intrinsic features of the flow. This paradigm shift hints at constraints that are physics-dependent. A lot of work has been done involving physics-based constraints for fluid motion estimation [12, 13, 25, 26, 27]. In [15], we have proposed a constraint-based refinement of optical flow. Using an image-driven evolutionary PDE model resulting from a quadratic regularization we have shown the well-posedness of such a refinement principle. An important characteristic of the model is the possibility of a diagonalization by the Cauchy-Riemann operator leading to a decoupled system involving diffusion of the curl and a multi-

plicative perturbation of the laplacian of the divergence of the flow. For a specific case, it was shown that the model is close to the physics-based model [25] using a modified augmented Lagrangian method.

A topic of major interest to the Computer Vision community is the performance evaluation methods for optical flow estimation. Several important contributions [4, 6, 7, 35] discuss robust methods for obtaining high accuracy flow fields. Motivated by the harmonic-constraint based regularization [36], we proposed a variational model for capturing rotational features and improving angular accuracy of the flow [16].

The current work proposes a unified framework that extends our previous methods in a nonlinear setting. The first model is a two-phase refinement process. A crude pixel correspondence is obtained in the first phase which constitutes a good starting solution. In the next phase, this estimate is refined using additional constraints. The second model estimates the flow directly in a single phase. The additional constraint is chosen motivated by the harmonic constraint-based regularization (see [36]). This approach replaces the oriented smoothness constraint with a weighted decomposition of divergence and curl of flow. We aim to capture the rotational features better by preserving edge information and improving the accuracy of the flow. Thus we consider only the curl component in our framework with an anisotropic weight term.

The total variation regularization leads to  $\Delta_1$ , the 1-Laplacian operator in the Euler-Lagrange equations. Obtaining a stable convergent scheme is a difficult task because of the singularity of the operator at the origin. As a result most of the implementation methods often yield slower algorithms. In this direction important contributions were made by Chambolle [9] and Zach [34]. Chambolle and Pock [10] proposed a first-order primal-dual algorithm for solving non-smooth convex optimization problems. This further opened up newer directions as a large class of problems in Image Processing and Computer Vision could be solved within this framework. In our work, we use the Chambolle-Pock algorithm for both of our models. The numerical implementation of the algorithm has two main steps, namely updating the primal variables by solving a system of equations at each iteration and updating the dual variables by computing the point-wise projection maps onto the unit ball. Both of these steps are computationally expensive. As a result the second model yields a slower algorithm with a convergence rate of order  $O(1/N^2)$ . By  $O(1/N^2)$  we mean if  $\epsilon$  is the error threshold then the number of iterations required to reach this threshold is  $1/\epsilon$ . The first model splits the above-mentioned steps in two-phases. This leads to a faster algorithm with a convergence rate of  $O(1/N)$ .

The organization of the paper is as follows. In Section (2) we give the general formulation and describe our model in detail. Next in Section (3), we study the mathematical well-posedness of our formulation using an evolutionary PDE approach. Subsequently, we employ the first-order primal-dual Chambolle-Pock algorithm to our models and derive the necessary optimality conditions in Section (4). We then discuss the implementation details, discretization of our models and

empirically demonstrate the nature of convergence in Section (5).

## 2 Our Model Description

Our general formulation is given as:

$$J(\mathbf{u}) = \int_{\Omega} \rho(\|f_t + \nabla f \cdot \mathbf{u}\|) + \alpha \sum_{i=1}^2 \int_{\Omega} \gamma(\|\nabla u_i\|) + \beta \int_{\Omega} \phi(x, f, \nabla f) \psi(\mathbf{u}, \nabla \mathbf{u}) \quad (2)$$

where  $\rho : \mathbb{R} \rightarrow \mathbb{R}$  is a function of the optical flow constraint,  $\gamma : \mathbb{R} \rightarrow \mathbb{R}$  governs the regularization of the flow. The functions  $\phi$  and  $\psi$  are chosen specific to applications. A summary of some of the variational models which belong to this framework is listed in the following table:

	$\rho(x)$	$\gamma(x)$	$\phi(x, f, \nabla f)$	$\psi(\mathbf{u}, \nabla \mathbf{u})$
Horn and Schunck[22]	$x^2$	$x^2$	0	0
Cohen[11]	$x^2$	$x$	0	0
Aubert[3]	$x$	$\sqrt{1+x^2}$	$c(x)$	$\mathbf{u}^2$
$L^1 - TV$ [34]	$x$	$x$	0	0
Our Model (M1)	0	$x$	$f^2$	$(\nabla \cdot \mathbf{u})^2$
Our Model (M2)	$x^2$	$x$	$\frac{\lambda^2}{\ \nabla f\ ^2 + \lambda^2}$	$(\nabla_H \cdot \mathbf{u})^2$

Table 1: Some choices for the functions

Based on the choice functions mentioned in the above table, the constraint-based refinement formulation becomes

$$(M1) \quad J(\mathbf{u}) = \alpha \sum_{i=1}^2 \int_{\Omega} \|\nabla u_i\| + \beta \int_{\Omega} f^2 (\nabla \cdot \mathbf{u})^2. \quad (3)$$

where  $\|\cdot\|$  is the Euclidean norm. Starting with  $\mathbf{u} = \mathbf{u}_0$ , where  $\mathbf{u}_0$  is the Horn and Schunck optical flow the above formulation obtains a refinement of  $\mathbf{u}_0$  driven by the additional constraint  $f \nabla \cdot \mathbf{u}$ . This term is the non-conservation term in the physics-based constraint due to non null-out of plane components [20]. This constraint preserves the spatial characteristics and vorticities of the flow. Thus this model can extract flow informations from fluid-based digital imagery much better.

From the choice functions, our second formulation is given as:

$$(M2) \quad J(\mathbf{u}) = \int_{\Omega} (f_t + \nabla f \cdot \mathbf{u})^2 + \alpha \sum_{i=1}^2 \int_{\Omega} \|\nabla u_i\| + \beta \int_{\Omega} \frac{\lambda^2}{\|\nabla f\|^2 + \lambda^2} (\nabla_H \cdot \mathbf{u})^2. \quad (4)$$

The additional constraint in this formulation is motivated by the harmonic-constraint based regularization discussed in [36]. By associating an anisotropic weight term with the curl in our formulation there are two main advantages. First, we are able to get a precise estimation of the infinitesimal rotation within the regions. Secondly, we achieve a better alignment of small vectors in the flow. This leads to an overall improvement in the endpoint error.

In either case, the choice of  $\phi$  decides the influence of the image term in the regularization process. If  $\phi = 1$ , then the additional constraint term in the functional is flow-driven, i.e. independent of the influence of the image data. The weight parameters  $\alpha, \beta$  play an important role in the regularization process. For rigid-body like motion which requires important edge-information to be preserved a higher value of  $\alpha$  is preferred. For fluid-based images where there is less edge-prominence, we choose a higher  $\beta$  value.

### 3 Well-Posedness

In this section we discuss the mathematical well-posedness of the proposed formulation. Let us denote  $\mathbf{u} = (u_1, u_2)$ . The space  $W^{1,p}(\Omega), p > 1$ , is the reflexive Banach space

$$W^{1,p}(\Omega) = \{u \in L^p(\Omega) : D^\alpha u \in L^p(\Omega), |\alpha| \leq 1\}$$

with the usual norm

$$\|u\|_{W^{1,p}} = \left( \sum_{|\alpha| \leq 1} \|D^\alpha u\|_{L^p}^p \right)^{1/p}, 1 \leq p < \infty.$$

To study the mathematical well-posedness of the proposed formulation we consider the following approximation.

$$J_{p,\mathbf{R}}(\mathbf{u}) = \beta \int_{\Omega} \phi(x, f, \nabla f) (\nabla \cdot \mathbf{u})^2 + \frac{\alpha}{p} \int_{\Omega} \{|\nabla u_1|^p + |\nabla u_2|^p\}, \quad 1 < p < 2 \quad (5)$$

This functional being strictly convex in  $W^{1,p}(\Omega)$  admits a unique minimizer. For this discussion we consider  $\phi(x, f, \nabla f) = f^2$ . The first important step is to show that  $J_{p,\mathbf{R}}$  converges to  $J_{1,\mathbf{R}}$  as  $p \rightarrow 1$ . For this, we refer to the discussion in Section 3.4 in [24].

**Lemma 1.**

$$\lim_{p \rightarrow 1} \frac{1}{p} \int_{\Omega} |\nabla u|^p = \int_{\Omega} |\nabla u|. \quad (6)$$

**Remark 1.** As  $J_{p,\mathbf{R}}(\mathbf{u}) \rightarrow J_{1,\mathbf{R}}(\mathbf{u})$ ,  $p \rightarrow 1$ , the corresponding Euler-Lagrange equations  $A_p = \Delta_p$  associated with the regularization term also converges to  $A_1 = \Delta_1$ .

**Remark 2.** The case  $p = 2$  leads to a linear diffusion-driven refinement process. The authors have previously studied and discussed this case in [15].

The associated parabolic system corresponding to the Euler-Lagrange equations of (5) are given as

$$\left\{ \begin{array}{l} \frac{\partial u_1}{\partial t} = \Delta_p u_1 + a_0 \frac{\partial}{\partial x} [f^2((u_1)_x + (u_2)_y)] \text{ in } \Omega \times (0, \infty), \\ \frac{\partial u_2}{\partial t} = \Delta_p u_2 + a_0 \frac{\partial}{\partial y} [f^2((u_1)_x + (u_2)_y)] \text{ in } \Omega \times (0, \infty), \\ u_1(x, y, 0) = u_1^0 \text{ in } \Omega, \\ u_2(x, y, 0) = u_2^0 \text{ in } \Omega, \\ u_1 = 0 \text{ on } \partial\Omega \times (0, \infty), \\ u_2 = 0 \text{ on } \partial\Omega \times (0, \infty), \end{array} \right. \quad (7)$$

where  $(u_1^0, u_2^0)$  is the starting feasible solution obtained by the Horn and Schunck optical flow,  $a_0 = 2\beta/\alpha$ . Rewriting the system in an abstract form leads us to

$$\left\{ \begin{array}{l} \frac{d\mathbf{u}}{dt} + \mathcal{A}_p \mathbf{u} = 0, \quad t > 0, \\ \mathbf{u}(0) = \mathbf{u}_0 \in H^1(\Omega)^2. \end{array} \right. \quad (8)$$

Here the operator  $\mathcal{A}_p = A_p + F$  where

$$A_p \mathbf{u} = - \begin{bmatrix} \Delta_p u_1 \\ \Delta_p u_2 \end{bmatrix}, \quad F \mathbf{u} = -a_0 \begin{bmatrix} \frac{\partial}{\partial x} [f^2((u_1)_x + (u_2)_y)] \\ \frac{\partial}{\partial y} [f^2((u_1)_x + (u_2)_y)] \end{bmatrix},$$

We will show that both the operators  $A_p$  and  $F$  are maximal monotone in  $W^{1,p}(\Omega) \cap L^2(\Omega)$  and  $L^2(\Omega)$  respectively.

**Lemma 2.** The operators  $A_p$  and  $F$  is maximal monotone in  $W^{1,p}(\Omega) \cap L^2(\Omega)$  and  $L^2(\Omega)$  respectively.

*Proof.* The maximal monotonicity of  $A_p$  follows directly from the discussions in [33]. To show monotonicity we show that  $\langle F \mathbf{u}, \mathbf{u} \rangle \geq 0$ . Indeed,

$$\begin{aligned} \langle F \mathbf{u}, \mathbf{u} \rangle &= -a_0 \int_{\Omega} \left\{ \frac{\partial}{\partial x} [f^2((u_1)_x + (u_2)_y)] u + \frac{\partial}{\partial y} [f^2((u_1)_x + (u_2)_y)] v \right\}, \\ &= a_0 \int_{\Omega} \{ f^2((u_1)_x + (u_2)_y) u_x + f^2((u_1)_x + (u_2)_y) v_y \}, \end{aligned}$$

$$= a_0 \int_{\Omega} f^2((u_1)_x + (u_2)_y)^2 \geq 0,$$

proving the monotonicity of  $F$ . To show the maximality we have to show that

$$\text{Ran}(I + F) = L^2(\Omega)^2, \quad (9)$$

i.e. there exists  $\mathbf{u}$  for all  $\mathbf{f} \in L^2(\Omega)^2$  such that  $\mathbf{u} + F\mathbf{u} = \mathbf{f}$  holds. Let  $\mathbf{f} = (f, g) \in L^2(\Omega)^2$  and consider the system

$$u + \frac{\partial}{\partial x}[f^2((u_1)_x + (u_2)_y)] = f,$$

$$v + \frac{\partial}{\partial y}[f^2((u_1)_x + (u_2)_y)] = g,$$

where  $f, g \in L^2(\Omega)$ . Applying the Cauchy-Riemann operator

$$R = \begin{bmatrix} \partial_y & -\partial_x \\ \partial_x & \partial_y \end{bmatrix}.$$

both sides we obtain the decoupled system

$$(u_1)_y - (u_2)_x = f_y - g_x, \quad (10)$$

$$(\Delta \circ k)((u_1)_x + (u_2)_y) = f_x + g_y \quad (11)$$

where  $k$  is the image-dependent multiplicative function  $k : f \mapsto 1 + a_0 f^2$ . The first equation (10) governs the curl of the flow  $\mathbf{u} = (u_1, u_2)$ . The second equation (11) indicates a non-homogeneous weighted diffusion process on the divergence with a weight  $k$ . Let us define  $h_1 = f_y - g_x$  and  $h_2 = f_x + g_y$ . Solving the second equation gives us an expression for the divergence of the flow. Let us call this as  $h_3$ . We thus obtain the following system

$$(u_1)_y - (u_2)_x = h_1,$$

$$(u_1)_x + (u_2)_y = h_3/k,$$

These are the inhomogeneous Cauchy-Riemann equations. In a compact form we rewrite them as

$$R\mathbf{u} = \tilde{\mathbf{f}}$$

where  $\tilde{\mathbf{f}} = (h_1, h_3/k)$ . The operator  $R^{-1}$  is a continuous operator of order -1 in the space  $W^{1,p}(\Omega)$ . Hence there exists a unique  $\mathbf{u}$  such that  $\mathbf{u} + F\mathbf{u} = \mathbf{f}$  holds. This concludes the proof.  $\square$

Now that we have shown the maximal monotonicity we define a function  $\Phi_p : L^2(\Omega)^2 \rightarrow (-\infty, +\infty]$  by

$$\Phi_p(\mathbf{u}) = \begin{cases} J_{p,\mathbf{R}}(\mathbf{u}), & \mathbf{u} \in [W^{1,p}(\Omega) \cap L^2(\Omega)]^2 \\ +\infty, & \mathbf{u} \in [L^2(\Omega) \setminus W^{1,p}(\Omega)]^2 \end{cases}.$$

Then clearly  $\Phi_p$  is convex and lower semi-continuous. Also  $\Phi_p$  is proper since  $D(\Phi_p) = D(A_p) \cap D(F) \neq \emptyset$ . Thus the associated subdifferential  $\partial\Phi(\mathbf{u}) \equiv \mathcal{A}_p$  is maximal monotone. Thus there is a unique solution  $\mathbf{u}$  of the inclusion

$$0 \in \mathbf{u}'(t) + \partial\Phi_p(\mathbf{u})$$

satisfying the initial conditions.

## 4 The Primal-Dual Framework

The primal-dual method is a numerical tool for solving optimization problems. The main idea is to replace a primal problem with an equivalent saddle point problem by introducing dual variables and employ efficient algorithms to obtain the desired convergence. In the recent past several saddle point frameworks have been proposed for variational problems in image processing and computer vision [10, 31, 35]. As our formulation involves non-smooth convex functionals, the most suitable framework is the one proposed by Chambolle and Pock [10]. Let  $\Omega \subset \mathbb{R}^2$  be an open, bounded set,  $\mathcal{X}, \mathcal{Y}$  be two finite-dimensional vector spaces with the scalar product  $(\cdot, \cdot)$  and the norm  $\|\cdot\|$ . Denote the primal variable  $\mathbf{u} = (u_1, u_2)$  and the dual variable  $\mathbf{d} = (d_1, d_2, d_3)$ . We first consider the variational problem in the following form

$$\arg \min_{\mathbf{u}} G(\mathbf{u}) + F(K\mathbf{u}). \quad (12)$$

where  $F, G : \mathcal{X} \rightarrow [0, \infty]$  are convex, proper and lower-semicontinuous functionals,  $K : \mathcal{X} \rightarrow \mathcal{Y}$  is a continuous, linear operator. The equivalent primal-dual formulation is given as

$$\arg \min_{\mathbf{u}} \arg \max_{\mathbf{d}} G(\mathbf{u}) + (K\mathbf{u}, \mathbf{d}) - F^*(\mathbf{d}). \quad (13)$$

where  $F^*$  is the convex conjugate of  $F$ . Table (2) gives a summary of each term of our model using the above notations. Given a  $\tau, \sigma > 0$ , an initial  $(\mathbf{u}^0, \mathbf{d}^0) \in \mathcal{X} \times \mathcal{Y}$ , the Chambolle-Pock algorithm solves the saddle point problem (13) by the following algorithm:

$$\mathbf{d}^{k+1} = \text{prox}_{\sigma F^*}(\mathbf{d}^k + \sigma K\bar{\mathbf{u}}^k),$$



$$\begin{aligned}\mathbf{u}^{k+1} &= \mathbf{prox}_{\tau G}(\mathbf{u}^k - \tau K^* \mathbf{d}^{k+1}), \\ \bar{\mathbf{u}}_{k+1} &= 2\mathbf{u}_{k+1} - \mathbf{u}_k \quad (\text{over-relaxation}),\end{aligned}$$

where

$$\mathbf{prox}_{\tau G}(\mathbf{d}) = (I + \tau \partial G)^{-1}(\mathbf{d}) = \arg \min_{\mathbf{u}} \left\{ \frac{1}{2} \|\mathbf{u} - \mathbf{d}\|^2 + \tau G(\mathbf{u}) \right\}$$

is the proximal or the resolvent operator. This can be thought of as a trade-off between minimizing  $G$  and being close to  $\mathbf{d}$ . We now employ the above algorithm for our problem and derive the necessary optimality conditions.

#### 4.1 Optimality Condition for Our Model (M1)

In this case we have

$$G(\mathbf{u}) = 0, \quad F(K\mathbf{u}) = \frac{1}{2} \int_{\Omega} f^2(\nabla \cdot \mathbf{u})^2 + \sum_{i=1}^2 \int_{\Omega} |\nabla u_i|.$$

The Operator  $K$  is given as

$$K\mathbf{u} = \begin{bmatrix} \nabla & 0 \\ 0 & \nabla \\ f^2 \partial_x & f^2 \partial_y \end{bmatrix} \begin{bmatrix} u_1 \\ u_2 \end{bmatrix}.$$

Therefore,

$$K^* \mathbf{d} = - \begin{bmatrix} \nabla \cdot & 0 & \partial_x(f^2 \cdot) \\ 0 & \nabla \cdot & \partial_y(f^2 \cdot) \end{bmatrix} \begin{bmatrix} d_1 \\ d_2 \\ d_3 \end{bmatrix}.$$

Using standard dual identities the convex conjugate  $F^*(\mathbf{d})$  is computed as

$$F^*(\mathbf{d}) = \frac{1}{2} \|d_3\|_2^2 + \alpha \sum_{i=1}^2 \delta_{B(L^\infty)}(d_i/\alpha),$$

where  $B(L^\infty)$  denotes the unit ball in  $L^\infty(\Omega)$  and

$$\delta_{B(L^\infty)}(x^*) = \begin{cases} 0, & \text{if } x^* \in B(L^\infty) \\ +\infty, & \text{otherwise} \end{cases}.$$

Model	$\phi(x, f, \nabla f)$	$G(\mathbf{u})$	$F(K\mathbf{u})$	$K$
Model (M1)	$f^2$	0	$\frac{1}{2} \int_{\Omega} \phi(x, f, \nabla f) (\nabla \cdot \mathbf{u})^2$ $+ \sum_{i=1}^2 \int_{\Omega}  \nabla u_i $	$\begin{pmatrix} \nabla & 0 \\ 0 & \nabla \\ \phi \partial_x & \phi \partial_y \end{pmatrix}$
Model (M2)	$\frac{\lambda^2}{\lambda^2 + \ \nabla f\ ^2}$	$\frac{1}{2} \int_{\Omega} (f_t + \nabla f \cdot \mathbf{u})^2$	$\frac{1}{2} \int_{\Omega} \phi(x, f, \nabla f) (\nabla_H \cdot \mathbf{u})^2$ $+ \sum_{i=1}^2 \int_{\Omega}  \nabla u_i $	$\begin{pmatrix} \nabla & 0 \\ 0 & \nabla \\ \phi \partial_y & -\phi \partial_x \end{pmatrix}$

Table 2: Summary of the terms in the Primal-Dual Formulation

Thus the primal-dual formulation is given as

$$\arg \min_{\mathbf{u}} \arg \max_{\mathbf{d}} (\mathbf{u}, K^* \mathbf{d}) - \frac{1}{2\beta} \|d_3\|_2^2 - \alpha \sum_{i=1}^2 \delta_{B(L^\infty)}(d_i/\alpha).$$

Accordingly, the Chambolle-Pock algorithm for this primal-dual problem is given as:

$$\begin{aligned} \tilde{\mathbf{d}}^{k+1} &= \mathbf{d}^k + \sigma K \bar{\mathbf{u}}, \\ \mathbf{d}_{1,2}^{k+1} &= \arg \min_{\mathbf{d}} \left\{ \frac{1}{2} \|\mathbf{d} - \tilde{\mathbf{d}}_{1,2}^{k+1}\|_2^2 + \alpha \sigma \delta_{B(L^\infty)}(\mathbf{d}/\alpha) \right\}, \\ d_3^{k+1} &= \arg \min_d \left\{ \frac{1}{2} \|d - \tilde{d}_3^{k+1}\|_2^2 + \frac{\sigma}{2\beta} \|d\|_2^2 \right\}, \\ \tilde{\mathbf{u}}^{k+1} &= \mathbf{u}^k - \tau K^* \mathbf{d}^{k+1}, \\ \bar{\mathbf{u}}_{k+1} &= 2\mathbf{u}_{k+1} - \mathbf{u}_k. \end{aligned}$$

To derive the optimality condition for the dual variables  $d_3$ , consider the functional

$$J(d_3) = \frac{1}{2} \int_{\Omega} (d_3 - \tilde{d}_3)^2 + \frac{\sigma}{2\beta} \int_{\Omega} d_3^2$$

Therefore setting  $d_\theta J = 0$  we get

$$d_3 - \tilde{d}_3 + \frac{\sigma}{\beta} d_3 = 0.$$

Rearranging we get

$$d_3^{k+1} = \frac{\beta}{\beta + \sigma} \tilde{d}_3^{k+1},$$

The solution for the indicator function  $\delta$  is given by the point-wise projections of  $\tilde{\mathbf{d}}^{k+1}$ ,  $\mathbf{proj}_\alpha(\tilde{\mathbf{d}}^{k+1})$  onto the unit ball, see [8, 17]. Thus the iterative scheme for the Chambolle-Pock is given as

$$\begin{aligned}\tilde{\mathbf{d}}^{k+1} &= \mathbf{d}^k + \sigma K \bar{\mathbf{u}}, \\ \mathbf{d}_{1,2}^{k+1} &= \mathbf{proj}_\alpha(\tilde{\mathbf{d}}_{1,2}^{k+1}), \\ d_3^{k+1} &= \frac{\beta}{\beta + \sigma} \tilde{d}_3^{k+1}, \\ \tilde{\mathbf{u}}^{k+1} &= \mathbf{u}^k - \tau K^* \mathbf{d}^{k+1}, \\ \bar{\mathbf{u}}_{k+1} &= 2\mathbf{u}_{k+1} - \mathbf{u}_k.\end{aligned}$$

## 4.2 Optimality Condition for Our Model (M2)

In this case we have

$$G(\mathbf{u}) = \frac{1}{2} \int_{\Omega} (f_t + \nabla f \cdot \mathbf{u})^2, \quad F(K\mathbf{u}) = \frac{1}{2} \int_{\Omega} \phi(f, \nabla f) (\nabla_H \cdot \mathbf{u})^2 + \sum_{i=1}^2 \int_{\Omega} |\nabla u_i|.$$

The Operator  $K$  is given as

$$K\mathbf{u} = \begin{bmatrix} \nabla & 0 \\ 0 & \nabla \\ \phi \partial_y & -\phi \partial_x \end{bmatrix} \begin{bmatrix} u_1 \\ u_2 \end{bmatrix}.$$

Therefore,

$$K^* \mathbf{d} = - \begin{bmatrix} \nabla \cdot & 0 & \partial_y(\phi \cdot) \\ 0 & \nabla \cdot & -\partial_x(\phi \cdot) \end{bmatrix} \begin{bmatrix} d_1 \\ d_2 \\ d_3 \end{bmatrix}.$$

As before, the convex conjugate  $F^*(\mathbf{d})$  is computed as

$$F^*(\mathbf{d}) = \frac{1}{2} \|d_3\|_2^2 + \alpha \sum_{i=1}^2 \delta_{B(L^\infty)}(d_i/\alpha),$$

Thus the primal-dual formulation is given as

$$\arg \min_{\mathbf{u}} \arg \max_{\mathbf{d}} \frac{1}{2} \int_{\Omega} (f_t + \nabla f \cdot \mathbf{u})^2 + (\mathbf{u}, K^* \mathbf{d}) - \frac{1}{2\beta} \|d_3\|_2^2 - \alpha \sum_{i=1}^2 \delta_{B(L^\infty)}(d_i/\alpha).$$

Accordingly, the Chambolle-Pock algorithm for this primal-dual problem is given as:

$$\begin{aligned}
\tilde{\mathbf{d}}^{k+1} &= \mathbf{d}^k + \sigma K \bar{\mathbf{u}}, \\
\mathbf{d}_{1,2}^{k+1} &= \arg \min_{\mathbf{d}} \left\{ \frac{1}{2} \|\mathbf{d} - \tilde{\mathbf{d}}_{1,2}^{k+1}\|_2^2 + \alpha \sigma \delta_{B(L^\infty)}(\mathbf{d}/\alpha) \right\}, \\
d_3^{k+1} &= \arg \min_d \left\{ \frac{1}{2} \|d - \tilde{d}_3^{k+1}\|_2^2 + \frac{\sigma}{2\beta} \|d\|_2^2 \right\}, \\
\tilde{\mathbf{u}}^{k+1} &= \mathbf{u}^k - \tau K^* \mathbf{d}^{k+1}, \\
\mathbf{u}^{k+1} &= \arg \min_{\mathbf{u}} \left\{ \frac{1}{2} \|\mathbf{u} - \tilde{\mathbf{u}}^{k+1}\|_2^2 + \frac{\tau}{2} \int_{\Omega} (f_t + \nabla f \cdot \mathbf{u})^2 \right\}, \\
\bar{\mathbf{u}}_{k+1} &= 2\mathbf{u}_{k+1} - \mathbf{u}_k.
\end{aligned}$$

The optimality conditions for the dual variables follow directly from above. For the primal variable  $\mathbf{u}$  the optimality condition can be obtained directly by a quadratic minimization, see [17] for more details. The equations are given as

$$\begin{aligned}
(1 + \tau f_x^2)u_1 + \tau f_x f_y u_2 &= \tilde{u}_1^{k+1} - \tau f_x f_t, \\
\tau f_x f_y u_1 + (1 + \tau f_y^2)u_2 &= \tilde{u}_2^{k+1} - \tau f_y f_t.
\end{aligned}$$

Thus the iterative scheme for the Chambolle-Pock is given as

$$\begin{aligned}
\tilde{\mathbf{d}}^{k+1} &= \mathbf{d}^k + \sigma K \bar{\mathbf{u}}, \\
\mathbf{d}_{1,2}^{k+1} &= \mathbf{proj}_{\alpha} \left( \tilde{\mathbf{d}}_{1,2}^{k+1} \right), \\
d_3^{k+1} &= \frac{\beta}{\beta + \sigma} \tilde{d}_3^{k+1}, \\
\tilde{\mathbf{u}}^{k+1} &= \mathbf{u}^k - \tau K^* \mathbf{d}^{k+1}, \\
\mathbf{u}^{k+1} &= \left( \frac{b_1 c_3 - c_2 b_2}{c_1 c_3 - c_2^2}, \frac{b_2 c_1 - c_2 b_1}{c_1 c_3 - c_2^2} \right), \\
\bar{\mathbf{u}}_{k+1} &= 2\mathbf{u}_{k+1} - \mathbf{u}_k.
\end{aligned}$$

where  $c_1, c_2, c_3$  are the elements of the coefficient matrix given by  $c_1 = 1 + \tau f_x^2, c_2 = \tau f_x f_y, c_3 = 1 + \tau f_y^2$ ,  $b_1, b_2$  are the right hand side values given by  $b_1 = \tilde{u}_1^{k+1} - \tau f_x f_t, b_2 = \tilde{u}_2^{k+1} - \tau f_y f_t$ . In the next section we will look at the numerical discretization and other implementation details.

## 5 Results

Having obtained the Chambolle-Pock algorithm for solving the saddle-point problem, we now look at the implementation details. Algorithm 1 shows the Chambolle-Pock algorithm for our nonlinear constraint-based refinement model.

---

### Algorithm 1

---

```

1: Initialize  $\tau, \sigma \leftarrow 1/\sqrt{8}, 1/\sqrt{8}$ 
2: Initialize  $\mathbf{u}^0 \leftarrow \text{HS}(f_1, f_2)$ ,  $\mathbf{d}^0 \leftarrow 0$ 
3: Initialize operator  $K$ 
4: repeat
5:    $\mathbf{u}_{\text{old}} \leftarrow \mathbf{u}$ 
6:   Build Matrix  $K$ 
7:    $\tilde{\mathbf{d}} \leftarrow \mathbf{d} + \sigma K \bar{\mathbf{u}}$ 
8:    $d_{1,2} \leftarrow \text{proj}_{\sigma/\alpha}(\tilde{d}_{1,2})$ 
9:    $d_3 \leftarrow \frac{\beta}{\beta+\sigma} \tilde{d}_3$ 
10:  Build Matrix  $K^*$ 
11:   $\tilde{\mathbf{u}} \leftarrow \mathbf{u} - \tau K^* \mathbf{d}$ 
12:   $\mathbf{u} \leftarrow \tilde{\mathbf{u}}$ 
13:   $\bar{\mathbf{u}} \leftarrow 2\mathbf{u} - \mathbf{u}_{\text{old}}$ 
14: until convergence

```

---

As mentioned previously this model works in two phases wherein the first phase we obtain a crude-pixel correspondence and subsequently refine this estimate in the next phase driven by additional constraints. The initial Horn and Schunck flow was computed using the Chambolle-Pock algorithm, see [10, 17]. Here we observed that using a forward difference scheme for both spatial and temporal image derivatives  $f_x, f_y$  and  $f_t$  respectively does not yield a stable discretization. Instead, a forward difference scheme for  $f_t$  and a central difference scheme for  $f_x, f_y$  does yield a stable numerical scheme. In the next step, the operator matrix  $K$  is constructed for updating the dual variables  $d_1, d_2, d_3$  shown in steps 9 and 10. This requires solving two sub-problems, one for  $d_1, d_2$  and the other for  $d_3$ .

Now  $\nabla u_i = (u_{i_x}, u_{i_y}), i = 1, 2$ . The associated dual variable is  $d_i = (d_{i,1}, d_{i,2})$ . The primal formulation had a total-variation regularization. Accordingly,

$$|\nabla u_i|_{L^1} = |u_{i_x}| + |u_{i_y}|.$$

Thus the associated dual norm for the variable  $d_i$  gives

$$\|d_i\|_{L^\infty} = \max\{|d_{i,1}|, |d_{i,2}|\}.$$

The solution for this minimization is the point-wise projection onto the unit ball corresponding to the dual norm. As shown previously, the convex conjugate of the

total variation term is the indicator function  $\delta_{L^\infty}(d_i/\alpha)$ . The associated convex set is defined by

$$\{d_i : \|d_i/\alpha\| \leq 1\} = \{d_i : \|d_i\| \leq \alpha\}, i = 1, 2.$$

Thus the dual update for  $d_{1,2}$  can be obtained by the point-wise projection of  $\tilde{d}_{1,2}$  onto  $[-\alpha, \alpha]$  given as

$$d_{1,2} = \mathbf{proj}_{\sigma/\alpha}(\tilde{d}_{1,2}) = \min(\alpha, \max(-\alpha, \tilde{d}_{1,2})).$$

The sub-problem for  $d_3$  is a linear quadratic minimization problem as discussed in the previous section. In the next step the adjoint operator  $K^*$  is constructed to update the primal variable  $\mathbf{u}$ . The subsequent over-relaxation step  $\bar{\mathbf{u}} \leftarrow 2\mathbf{u} - \mathbf{u}_{\text{old}}$  is a particular case for  $\theta = 1$  in [10] for easier estimates of the convergence. The algorithm is further simplified if the regularization term is linear. In this case the only difference that occur is the updation of the dual variable  $d_{1,2}$  leading to the optimality condition

$$d_{1,2} = \frac{\alpha}{\alpha + \sigma} \tilde{d}_{1,2}.$$

The stopping criterion is determined by computing the normalized error from the primal and dual residues. This error metric was introduced by the authors in [18] and is numerically less expensive. Let  $\mathbf{u}^{(k)}, \mathbf{d}^{(k)}$  be the primal and the dual updates after  $k$  iterations respectively. Then the primal and dual residues at the  $k^{\text{th}}$  iteration are computed by the formula:

$$\begin{aligned} p_{\text{res}}^{(k)} &:= \left| \frac{\mathbf{u}^{(k)} - \mathbf{u}^{(k+1)}}{\tau} - K^*(\mathbf{d}^{(k)} - \mathbf{d}^{(k+1)}) \right|, \\ d_{\text{res}}^{(k)} &:= \left| \frac{\mathbf{d}^{(k)} - \mathbf{d}^{(k+1)}}{\sigma} - K(\mathbf{u}^{(k)} - \mathbf{u}^{(k+1)}) \right|. \end{aligned}$$

Therefore the normalized error at  $k^{\text{th}}$  step is obtained as:

$$e^{(k)} = \frac{p_{\text{res}}^{(k)} + d_{\text{res}}^{(k)}}{\mu(\Omega)},$$

where  $\mu(\Omega)$  refers to the measure of the domain  $\Omega$ . Chambolle and Pock [10] also showed that the convergence criterion is fulfilled when  $\tau\sigma\|K\|^2 < 1, \theta = 1$ . Thus  $\tau$  and  $\sigma$  needs to be chosen accordingly. An optimal numerical upper-bound was obtained by Chambolle [9] which satisfies the above criterion. Accordingly we set  $\tau = \sigma = 1/\sqrt{8}$ .

The Chmabolle-Pock algorithm for the angular accuracy model follows in a similar manner. The main difference lies in the primal update step 13 because of the explicit presence of the data term in the functional. The subroutine *solvePrimal* up-

dates the primal variable  $\mathbf{u}$  by solving a quadratic minimization problem discussed previously leading to the following update step,

$$\mathbf{u}^{k+1} = \left( \frac{b_1 c_3 - c_2 b_2}{c_1 c_3 - c_2^2}, \frac{b_2 c_1 - c_2 b_1}{c_1 c_3 - c_2^2} \right),$$

where  $c_1 = 1 + \tau f_x^2$ ,  $c_2 = \tau f_x f_y$ ,  $c_3 = 1 + \tau f_y^2$ ,  $b_1 = \tilde{u}_1^{k+1} - \tau f_x f_t$ ,  $b_2 = \tilde{u}_2^{k+1} - \tau f_y f_t$ . We now show the results for obtained by implementing the algorithm. The first sequence is the Oseen vortex pair. For more details on the sequence we refer to [25].

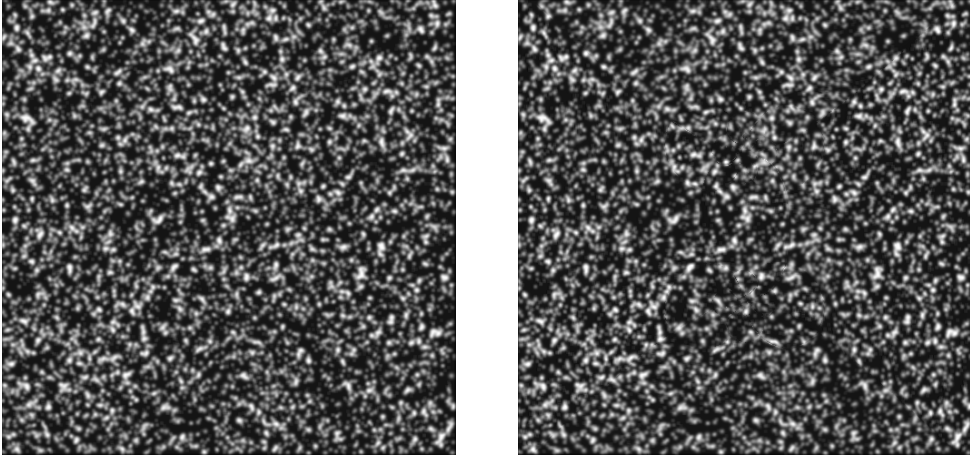


Figure 1: Oseen Vortex Pair [25].

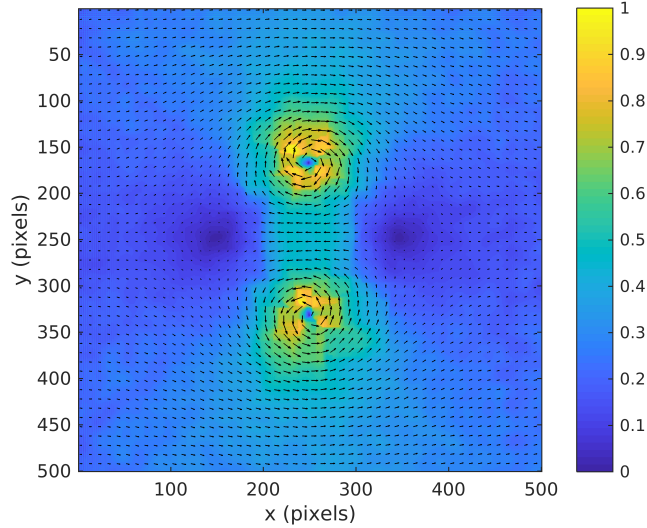


Figure 2: Velocity magnitude plot for the Oseen vortex pair.

Figure (2) shows the velocity magnitude plot obtained for the oseen vortex pair. The algorithm produces dense flow fields while correctly estimating the vortex cores.

We set  $\alpha = 0.1$  and  $\beta = 0.01$  and the algorithm was run for 50 iterations. We now empirically demonstrate the rate of convergence of both models.

	Model 1	Model 2
Oseen Vortex Pair	755	53753
Cloud Sequence	450	16068
Sphere Sequence	561	18009
Hydrangea	937	12574
Rubberwhale	617	13590

Table 3: Total number of iterations required by the algorithms to reach the threshold of  $10^{-2}$ .

Table (3) shows the number of iterations required by the algorithm to reach the error threshold of  $10^{-2}$ . The results indicate that the two-phase refinement process yields significantly faster convergence than the single-phase model.

## 5.1 Modern Implementation Principles

Recent developments in optical flow computation reveal that the flow estimates can be significantly improved by incorporating certain principles. To accommodate these principles in our framework Algorithm 1 is suitably modified to make it a part of a larger implementation procedure.

The computation of image derivatives follows a weighted averaging principle [29, 7]. The current flow estimates are used to warp the second image towards the first using bi-cubic interpolation. The time derivative is the difference between the first image and the warped image. The spatial derivatives are obtained as a weighted average of the first image and the warped image. The weight coefficient is called the blending ratio was chosen between 0 and 1.



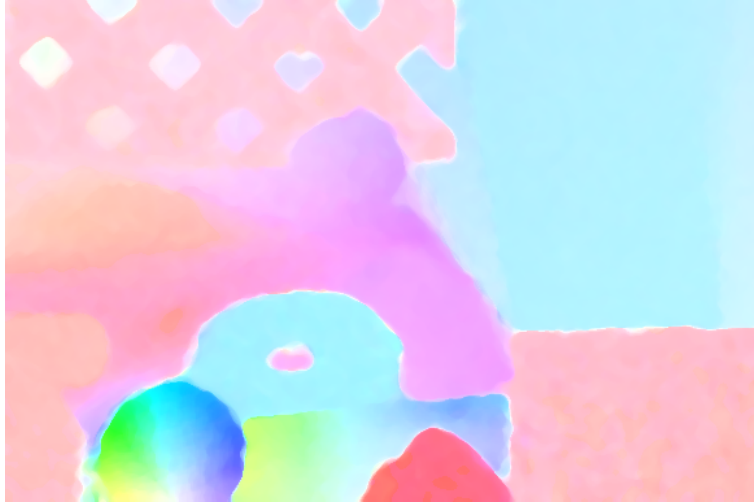


Figure 3: Estimated flow field for the *rubberwhale* sequence.

To account for large displacements of pixel motions, a coarse-to-fine pyramidal scheme is employed [32, 7, 17]. The flow field is first computed at the coarsest level. This estimate is upsampled to the next finer level via interpolation and is used to warp the second image towards the first image. The flow increments at this finer level are then computed between the first image and the warped image. This process continues till the finest resolution level is reached. At each pyramid level, 10 warping steps are performed. after each warping iteration, a  $5 \times 5$  median filter is applied on the flow estimates to remove outliers. Figure (3) shows the obtained flow field for nonlinear refinement using Algorithm 1 for the rubberwhale sequence.

	Algorithm 1 <sup>†</sup>	
	<b>AAE</b>	<b>EPE</b>
Linear Refinement	3.412	0.10
Nonlinear Refinement	3.347	0.103

Table 4: Comparison of the Average Angular Error (AAE) and End Point Error (EPE) for *rubberwhale* sequence. (<sup>†</sup> refers to the algorithm incorporated with the modern implementation principles)

An improvement is seen in the average angular error (AAE) and the end-point error (EPE) for the nonlinear refinement compared to the linear refinement for the *rubberwhale* sequence as shown in Table (4). For these experiments we set  $\alpha = 10, \beta = 1$ . The next experimental dataset is the sphere sequence [2].

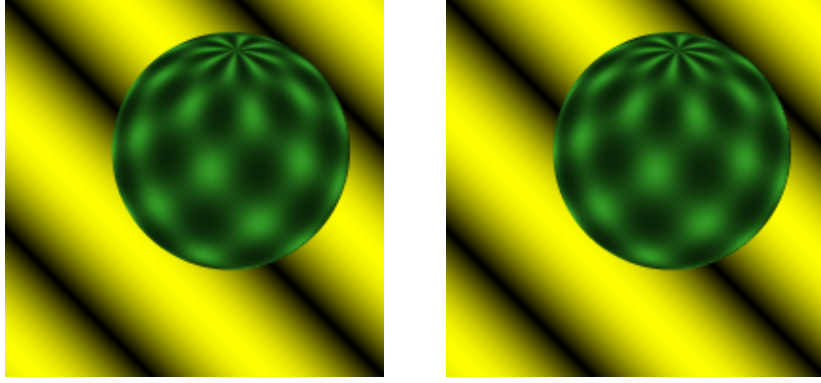


Figure 4: Sphere sequence [2]



(a) Linear Refinement



(b) Nonlinear Refinement

Figure 5: Estimated flow fields of the *sphere* sequence from [2] using Algorithm 1.

Figure (5) shows the color-coded flow estimate for the *sphere* sequence using the Middlebury color coding. The isotropic behaviour is seen in the linear case because of which the edges are not well preserved. The experiments were performed with  $\alpha = 1, \beta = 0.1$ .

**Acknowledgements.** The authors dedicate this paper to Bhagawan Sri Sathya Sai Baba, Revered Founder Chancellor, SSSIHL.

## References

- [1] <https://vision.middlebury.edu/flow/data/>

- [2] <http://of-eval.sourceforge.net/>
- [3] Aubert G., Deriche R., Kornprobst P.: Computing Optical Flow via Variational Techniques, *SIAM Journal of Applied Mathematics*, Vol. 60, 156-182 (1999).
- [4] Barron J.L., Fleet J., Beauchemin S., Performance of Optical Flow Techniques, *International Journal of Computer Vision*, 12(1), 43-77 (1994).
- [5] Brezis H., *Functional Analysis, Sobolev Spaces and Partial Differential Equations*, Springer, New York (2011).
- [6] Brox T., Bruhn A., Papenberg N., Weickert J., High Accuracy Optical Flow Estimation Based on a Theory of Warping, *European Conference of Computer Vision*, 25-36 (2004).
- [7] Bruhn A., Weickert J., Towards Ultimate Motion Estimation: Combining Highest Accuracy with Real-time Performance, *Tenth IEEE International Conference on Computer Vision*, Vol. 1, 749-755 (2005).
- [8] Burger M., Dirks H., Frerking L., On Optical Flow Models for Variational Motion Estimation In: M. Bergounioux, G. Peyré, C. Schnörr, J. Caillaud & T. Haberorn (Ed.), *Variational Methods: In Imaging and Geometric Control*, Berlin, Boston: De Gruyter, 225-251 (2017).
- [9] Chambolle A., An Algorithm for Total Variation Minimization and Applications, *Journal of Mathematical Imaging and Vision*, 20, 89-97 (2004).
- [10] Chambolle A., Pock T., A First-Order Primal-Dual Algorithm for Convex Problems with Applications in Imaging, *Journal of Mathematical Imaging and Vision*, 40, 120-145 (2011).
- [11] Cohen I., Nonlinear Variational Method for Optical Flow Computation, *Proceedings of the 8th SCIA*, 523-530 (1993).
- [12] Corpetti T., Mémmin E., Pérez P.: Estimating Fluid Optical Flow, *Proceedings of the 15th International Conference on Pattern Recognition, ICPR-2000*, Vol. 3, 1033-1036 (2000).
- [13] Corpetti T., Heitz D., Arroyo G., Mémmin E., Santa-Cruz A.: Fluid Experimental Flow Estimation based on an Optical Flow Scheme, *Experiments in Fluids*, (2006).
- [14] Dirks H., *Variational Methods for Joint Motion Estimation and Image Reconstruction*, Ph.D. Thesis, Wilhems-Universität (2015).
- [15] Doshi H, N. Uday Kiran: Constraint-Based Refinement of Optical Flow, <https://arxiv.org/abs/2011.12267>.

- [16] Doshi H., N. Uday Kiran, A Variational Optical Flow Model for Improving Angular Accuracy, <https://arxiv.org/abs/2102.00487>.
- [17] Dirks H., Variational Methods for Joint Motion Estimation and Image Reconstruction, Ph.D. Thesis, Wilhems-Universität (2015).
- [18] Goldstein T., Esser E., Baraniuk R., Adaptive Primal-Dual Hybrid Gradient Methods for Saddle-Point Problems, [arXiv:1305.0546](https://arxiv.org/abs/1305.0546) (2013).
- [19] Hauer D., Mazon J.: Regularizing effects of homogeneous evolution equations: the case of homogeneity of order zero, *Journal of Evolution Equations*, 19, 965-996 (2019).
- [20] Heitz D., Mémin E., Schnörr C.: Variational Fluid Flow measurements from Image Sequences: Synopsis and Perspectives, *Experiments in Fluids*, 48, 369-393 (2010).
- [21] Hinterberger W., Scherzer O., Schnörr C., Weickert J.: Analysis of Optical Flow Models in the Framework of Calculus of Variations, *Numer. Funct. Anal. and Optimiz.*, 23(1&2), 69-89 (2002).
- [22] Horn B.K.P., Schunck B.G.: Determining Optical Flow, *Artificial Intelligence*, Vol. 17, 185-203 (1981).
- [23] Kumar A., Tannenbaum A., Balas G., Optical flow: A curve evolution approach, *IEEE Transactions of Image Processing* 5, 598-611 (1996).
- [24] Martin A., Schiavi E., de Léon S.S.: On 1-Laplacian elliptic equations modeling magnetic resonance imaging Rician denoising, *Journal of Mathematical Imaging and Vision*, 57:202-224 (2017).
- [25] Liu T.: OpenOpticalFlow: An Open Source Program for Extraction of Velocity Fields from Flow Visualization Images, *Journal of Open Research Software*, 5:29 (2017).
- [26] Liu T., Shen L.: Fluid Flow and Optical Flow, *Journal of Fluid Mechanics*, 614, 253-291 (2008).
- [27] Luttmann A., Bollt E.M., Basnayake R., Kramer S., Tufillaro N.B.: A Framework for Estimating Potential Fluid Flow from Digital Imagery, *Chaos: An Interdisciplinary Journal of Nonlinear Science*, Vol. 23, 3 (2013).
- [28] Schnörr C.: Determining optical flow for irregular domains by minimizing quadratic functionals of a certain class, *International Journal of Computer Vision*, Vol. 6, 25-38 (1991).

- [29] Sun D., Roth R., Black M.J., Secrets of Optical Flow Estimation and their Principles, IEEE Computer Society Conference on Computer Vision and Pattern Recognition, 2432-2439 (2010).
- [30] Sun, D., Roth, S., Black, M. J., A Quantitative Analysis of Current Practices in Optical Flow Estimation and the Principles Behind them, International Journal of Computer Vision, 106(2), 115-137 (2014).
- [31] Zhang X., Burger M., Osher S., A Unified Primal-Dual Algorithm Framework Based on Bregman Iteration, Journal of Scientific Computing, 46, 20-46 (2011).
- [32] Wedel A., Pock T., Zach C., Cremers D., Bischof H., An Improved Algorithm for TV- $L^1$  Optical Flow, Dagstuhl Motion Workshop (2008).
- [33] Wei L., Agarwal R. P., Wong P.J.Y.: Existence and iterative construction of solutions to non-linear Dirichlet boundary value problems with  $p$ -Laplacian operator, Complex Variables and Elliptic Equations: An International Journal, 55:5-6, 601-608 (2010).
- [34] Zach C., Pock T., Bischof H., A Duality Based Approach for Realtime TV- $L^1$  Optical Flow, LNCS 4713, 214-223, DAGM (2007).
- [35] Zhang B., Zhu Z., A Primal-Dual Algorithm Framework for Convex Saddle-Point Optimization, Journal of Inequalities and Applications, 267 (2017).
- [36] Zhao J., Wang Y., Wang H., Optical flow with Harmonic Constraint and Oriented Smoothness, Sixth International Conference on Image and Graphics, 94-99 (2011).